Optical Fiber Technology **5,** 305–330 (1999)
Article ID ofte.1998.0279, available online at http://www.idealibrary.com on IDEAL®

Invited Paper

Photonic Crystal Fibers: A New Class of Optical Waveguides

Jes Broeng

Department of Electromagnetic Systems, Technical University of Denmark, Building 348, DK-2800 Lyngby, Denmark
E-mail: jb@emi.dtu.dk

Dmitri Mogilevstev

Optoelectronics Group, School of Physics, University of Bath, Claverton Down, Bath, BA2 7AY, United Kingdom

and

Stig E. Barkou and Anders Bjarklev

Department of Electromagnetic Systems, Technical University of Denmark, Building 348, DK-2800 Lyngby, Denmark

Received September 9, 1998

Remarkable properties of optical fibers with a high-index core region and a surrounding silica/air photonic crystal cladding have recently been reported. Here we discuss the physics, the special guiding properties, and the theoretical tools developed for the modeling of these photonic crystal fibers. With an emphasis on the applicational aspects of the fibers, we study their single-mode operation, bending losses, and dispersion properties. While exhibiting certain unique properties, the high-index core photonic crystal fibers share many common features with conventional optical fibers, attributed to an operation based on the well-known mechanism of total internal reflection. Fundamentally different from all high-index core fibers, in this work we demonstrate a novel type of optical waveguide, operating truly by the photonic bandgap effect. The novel fiber has an improved photonic crystal cladding and a central *low-index* structural defect along which the light is guided. The novel fiber has several unique features due to its different waveguidance mechanism, including remarkable dispersion

1068-5200/99 $30.00

properties and the potential to localize part of the guided mode in air regions. The results presented are fundamental in the field of photonic bandgap guidance, and this new class of optical waveguide is, therefore, expected to be of future interest to a large variety of research areas.

I. INTRODUCTION

Optical fibers and integrated optical waveguides are today finding wide use in areas covering telecommunications, sensor technology, spectroscopy, and medicine [1]. Their operation usually relies on light being guided by the physical mechanism known as total internal reflection (TIR), or index guiding. In order to achieve TIR in these waveguides (which are formed from dielectrics or semiconductors), a higher refractive index of the core compared to the surrounding media is required. TIR is a physical mechanism that has been known and exploited technologically for many years. However, within the past decade the research in new purpose-built materials has opened up the possibilities of localizing and controlling light in cavities and waveguides by a new physical mechanism, namely the photonic bandgap (PBG) effect [2–9].

The PBG effect may be achieved in periodically structured materials having a periodicity on the scale of the optical wavelength. Such periodic structures are usually referred to as photonic crystals, or photonic bandgap structures. By appropriate choice of crystal structure, the dimensions of the periodic lattice, and the properties of the component materials, propagation of electromagnetic waves in certain frequency bands (the photonic bandgaps) may be forbidden within the crystal. This ability of photonic crystals to inhibit the propagation of photons with well-defined frequencies has a close analogy with the electronic properties of semiconductors [10, 11]. This fact has caused a tremendous interest in photonic crystals, and their utilization has been predicted to have a major impact on a wide range of photonics applications [12–15]. Furthermore, the scalability of the electromagnetic properties of photonic crystals allows them to be exploited over the whole electromagnetic spectrum, covering optical to microwave frequencies [16–18].

A special class of components incorporating photonic crystals are optical fibers (or waveguides) with a two-dimensional (2D) periodic variation in the plane perpendicular to the fiber axis and an invariant structure along it. We refer to such structures as photonic crystal fibers (PCF) [19]. Within the past few years Russell and co-workers have pioneered this field by the realization of PCFs, compromising fine silica fibers with an array of air holes running down their length (see Fig. 1) [19–23]. This microstructured fiber has recently been used to form waveguides with new propagation properties, compared to conventional optical fibers. We will address these properties here, as well as the presently used tools for their modeling.

Although these new waveguides show remarkable properties, it is important to notice that they have a core, with a refractive index above the effective index of the surrounding material, and the waveguidance is caused by TIR. The realization of a fiber that truly operates by the photonic bandgap effect would naturally be of great

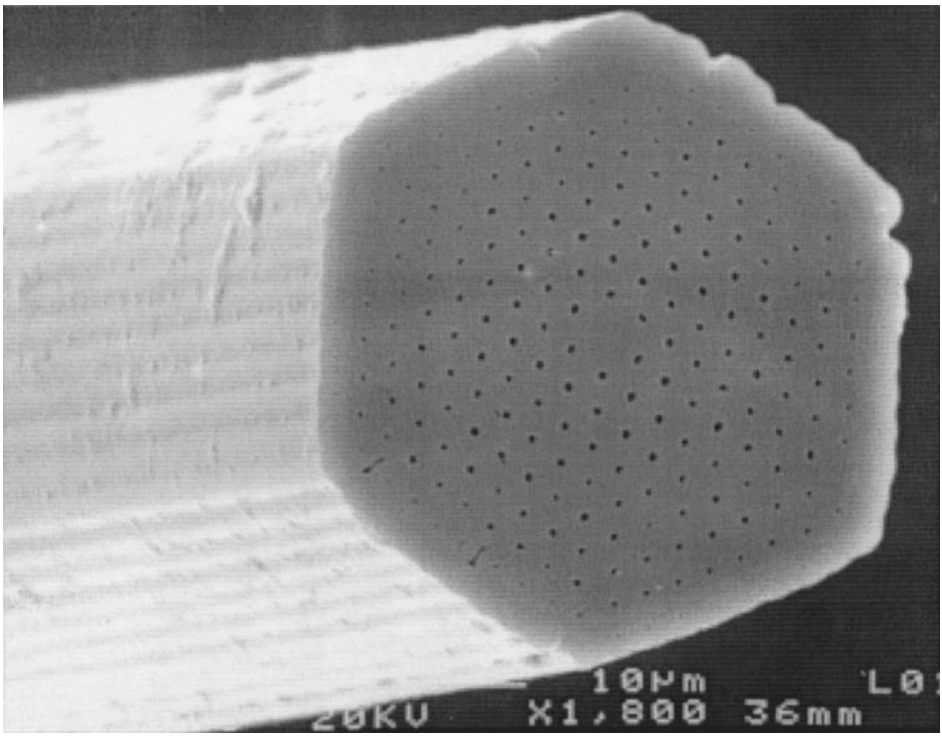

FIG. 1. Photonic crystal fiber, currently fabricated at the University of Bath [23].

interest from both a fundamental and an application-oriented point of view. For the triangular-based cladding structure used for the PCFs, it has proven difficult to realize a structure exhibiting PBG effect at optical wavelengths. We have thus turned our interest toward different crystal structures. This search for new structures has proven to be very fruitful and has led to the development of a new PCF design [24, 25]. We here present an investigation of this novel PCF, which appears immediately realizable. It thus seems very promising for achieving the goal of experimental realizations of new optical fibers, guiding light by a mechanism different from that of all former fibers.

The paper is organized in the following way. In Section II we present three different methods currently applied for the modeling of PCFs. The properties of the index guiding PCFs are discussed in Section III, and in Section IV we investigate new photonic crystal cladding structures and explain the principles for waveguiding by the PBG effect. The novel PCF design is presented, and its flexibility and possibilities of improving and adding to today's fiber applications are discussed.

II. MODELING PHOTONIC CRYSTAL FIBERS

The complex nature of the cladding structure of the PCFs does not allow for the direct use of methods from traditional fiber theory. Especially for the novel PCF, operating by the PBG effect, the full vectorial nature of the electromagnetic waves

has to be taken into account, and a method closely related to the plane-wave methods used for calculating electronic bandgaps in semiconductors has been developed. However, for the index-guiding PCFs, a simpler scalar model, based on an effective-index of the cladding, has proven to give a good qualitative description of the operation. We will be using this model to gain qualitative information about the properties of the high-index core triangular PCFs, as well as a more advanced method, based on the direct solution of Maxwell's equations around the core region of the triangular PCF using a set of localized basis functions, for accurately determining the modal dispersion properties.

A. *Effective-Index Approach*

In order to establish a relatively simple numerical tool that could provide qualitative mode-propagation properties of the high-index core triangular PCFs, Birks *et al*. [26] proposed a method in which sequential use of well-established fiber tools was applied. The fundamental idea behind this work was to first evaluate the periodically repeated hole-in-silica structure of the cladding and then (based on the approximate waveguiding properties of this cladding structure) replace the cladding by a properly chosen effective index. In this model, the resulting waveguide then consists of a core and a cladding region that have refractive indices n_{co} and n_{cl}, respectively. The core is pure silica, but the definition of the refractive index of the microstructured cladding region is given in terms of the propagation constant of the lowest-order mode that could propagate in the infinite cladding material. We will now briefly review this scalar effective-index method, which also has been used as a basis for the approximate dispersion and bending analysis presented in [27] and elaborated on in Section IIIB of this paper.

The first step of the effective-index method is to determine the cladding mode field, Ψ, by solving the scalar-wave equation within a simple cell centered on one of the holes. The diameter of these cells equals the pitch, Λ, between the holes of the cladding structure, and as illustrated in Fig. 2, their hexagonal shapes have been approximated by a circular one in order to make a general circular symmetric mode solution possible. By reflection symmetry, the boundary condition at the cell edge (at radius $\Lambda/2$) is $d\Psi/ds = 0$, where s is the coordinate normal to the edge. This means that in the corners of the original hexagonal-shaped cells we have to imagine constant fields with values equal to those at the circular cell boundary. The propagation constant of the resulting fundamental space-filling mode, β_{fsm}, is used to define the effective index of the cladding as $n_{\mathrm{eff}} = \beta_{\mathrm{fsm}}/k$ (where k is the free-space propagation constant of light with wavelength λ). Figure 2 further shows an example of the resulting field distribution in the cladding cell. It should also be noted that in the calculation of this cladding field (together with the effective-index value) we have used the normal weakly guiding field assumption [28], although the index step between the central hole (refractive index 1.0) and the surrounding silica (refractive index around 1.45) actually is considerable. However, the hereby introduced inaccuracy is considered to be less significant than the approximation of the

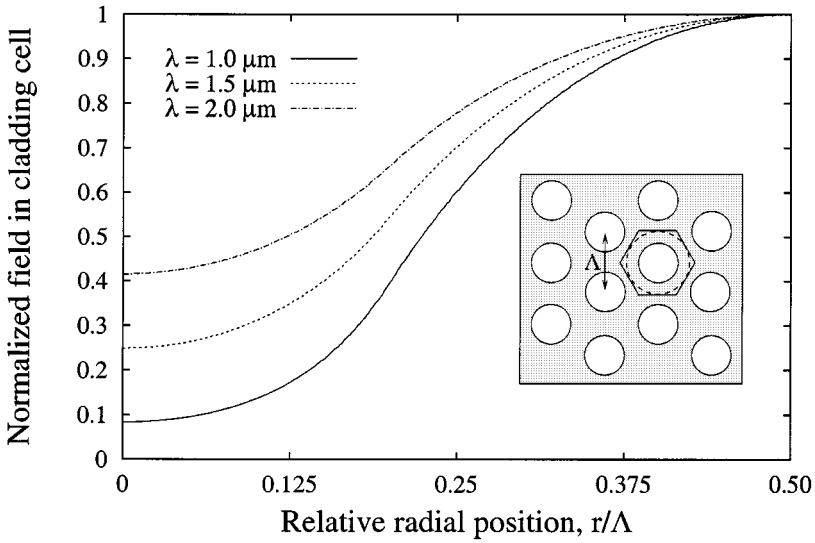

FIG. 2. Mode distributions in cladding cell for a silica PCF with a pitch of 2.3 μm, and an air-hole size given by $d/\Lambda = 0.40$ (fiber parameters comparable to those presented by Birks *et al.* in [26]). The modes are calculated at wavelengths 1.0, 1.5, and 2.0 μm. Inset shows the hexagonally shaped cladding cell with its inscribed circular approximation. A slightly different circular approximation was used in [26].

guided-mode field in the effective-index fiber compared to the actual field in the PCF.

Now having determined the cladding- and core-index values, we may calculate the approximate propagation properties of the PCF as for a step-index fiber with core index n_{co}, core radius $\Lambda/2$, and cladding index $n_{cl} = n_{eff}$. As an extension to the cladding-mode model originally described in [26], it was in [27] added that the refractive index for silica was wavelength dependent. This was done through the introduction of the generally applied Sellmeier formula [29]. In Section IIIB, the effective-index model will be used for an investigation of bending loss and dispersion properties.

B. *The Method of Localized Basis Functions*

Despite the good qualitative information provided by the simple effective-index model, advanced numerical methods must be used for highly accurate modeling of the PCFs. A method based on the direct solution of Maxwell's equations, using a representation of the refractive index and the field distributions as sums of localized basis functions, has recently been developed for the modeling of triangular PCFs [30]. Here, we will review the method, and in Section IIIA we apply it to the calculation of single-mode operation and group velocity dispersion of triangular PCFs.

The guided modes of the PCFs are localized in the close vicinity of the defect forming the core. Therefore, it is possible to model the guided modes by representing the fields as sums of functions localized in the vicinity of the core. A clear

advantage of such an approach is that for an appropriately chosen set of basis functions, only a modest number of functions are required to accurately describe the bound mode, thereby significantly lowering the demand for computational resources. To implement the method we reformulate Maxwell's equations for a medium translationally invariant along the z axis as an eigenvalue problem for the propagation constant β [31],

$$\left(\nabla_\perp^2 + k^2\varepsilon\right)\mathbf{h}_\perp + \left(\nabla_\perp \ln(\varepsilon)\right) \times \left(\nabla_\perp \times \mathbf{h}_\perp\right) = \beta^2 \mathbf{h}_\perp , \tag{1}$$

where $\nabla_\perp$ denotes the gradient in the periodic xy plane, k is the free-space wave number, and the components of the vector $\mathbf{h}_\perp = [h_x h_y]^T$ correspond to the transversal components of the magnetic field $\mathbf{H}$,

$$H_i = h_i \exp\left[i(\beta z - ck_0 t)\right]; \qquad i = x, y.$$

For the system of basis functions we used the set of Hermite–Gaussian functions [30]

$$\phi_{mn} = \exp\left[-\left(x^2 + y^2\right)/2\Lambda^2\right] \mathscr{H}_m(x/\Lambda)\mathscr{H}(y/\Lambda), \tag{2}$$

where $\mathscr{H}_m$ is the Hermite polynomial of the order m and Λ denotes the period of the lattice. The functions ϕ_{mn} are mutually orthogonal and form a complete system in the xy plane. They are localized in the vicinity of the point $x, y = 0$. In the basis of functions $\phi_{m,n}$ Eq. (1) becomes the algebraic eigenvalue problem

$$\sum_{kl} L_{k,l}^{m,n} \mathbf{h}_\perp^{k,l} = \beta^2 \mathbf{h}_\perp^{m,n} \tag{3}$$

for the vector of coefficients $\mathbf{h}_\perp^{k,l}$ representing the transversal magnetic field in the Hermite–Gaussian basis. $L_{k,l}^{m,n}$ are the matrix coefficients of the operator on the left-hand side of Eq. (1) in the Hermite–Gaussian basis. They are real and may be found analytically for a wide range of lattices.

The implementation of the method becomes especially simple in the high-frequency regime, where the coupling between the orthogonal components of the field in the transversal plane becomes negligible. In this regime, a scalar approximation holds, and the eigenvalue problem (3) becomes Hermitian. For calculations of the guided modes of the PCFs, the third term in Eq. (1), describing the coupling between the orthogonal components of the field in the transversal plane, scales with the air filling fraction, and for small holes the high-frequency limit is reached very quickly. For example, triangular PCFs with an air filling fraction less than 10% are in the high-frequency regime for wavelengths less than Λ.

C. *Full-Vectorial Plane-Wave Expansion Method*

For the general calculation of photonic bandgaps in full periodic structures and the modes introduced by structural defects, various methods have been proposed [32–37]. One of the most widely used is the plane-wave method [32]. This method solves the full-vector wave equation for the magnetic field and, as the name

implies, is based on a plane-wave expansion of the field and an expansion of the position-dependent dielectric constant. The method has a very general nature for treating periodic structures and may be applied to one-, two-, and three-dimensional problems. It allows one to calculate the photonic band diagrams of photonic crystals and thereby the possible existence, width, and positioning of any PBGs. By an enhancement of the simple plane-wave method, it may also be used to treat the important case of structural defects in the photonic crystal. This is the method we will be employing in Section IV for the analysis of the novel PCF.

For a single mode, the full-vector wave equation of the magnetic field $H_{\mathbf{k}}$ may be obtained from Maxwell's equations and expressed as

$$\nabla \times \left[\frac{1}{\varepsilon(r)} \nabla \times H_{\mathbf{k}} \right] = -\frac{\omega^2}{c^2} H_{\mathbf{k}}, \tag{4}$$

where $\mathbf{k}$ represents the wave propagation vector of the mode and $\varepsilon(r)$ is the position-dependent dielectric constant of the periodic structure. Taking advantage of the periodic nature of the problem, the H-field may be expanded into a sum of plane waves using Bloch's theorem as

$$H_{\mathbf{k}} = \sum_G h_{\mathbf{k}-\mathbf{G}} \exp(-i(\mathbf{k} - \mathbf{G}) \cdot \mathbf{r}), \tag{5}$$

where G represents a lattice vector in reciprocal space, describing the periodic structure. The dielectric constant may be expressed as a Fourier series expansion

$$\frac{1}{\varepsilon(r)} = \sum_G V_G \exp(iG \cdot r), \tag{6}$$

where

$$V_G = \frac{1}{A_u} \int \frac{1}{\varepsilon(r)} \exp(-iG \cdot r)\, dr. \tag{7}$$

In (7), A_u indicates the area of a unit cell, i.e., the smallest region, that may be used to represent the periodic structure. In Section IV we will look in greater detail at the special unit cells applied for the modeling of PCFs. Finally, by substituting (5) and (6) into (4) a matrix eigenvalue problem is obtained, where, for a fixed wave vector, $\mathbf{k}$, the frequencies, ω, of the allowed modes in the periodic structure are found as eigenvalues.

III. INDEX-GUIDING PCFS

Due to an operation based on total internal reflection, the properties of high-index core triangular PCFs in many respects resemble those of step-index fibers. However, very important differences occur as a result of the complex geometry of the cladding structure. In this section we address some of the basic waveguiding properties of the PCFs and compare them to standard optical fibers.

Second, we look at some of their more advanced properties which have a direct application-oriented interest.

A. *Basic Properties*

Similar to standard optical fibers, the high-index core triangular PCFs will always support at least one index-guided mode. In Fig. 3, we have illustrated the field distribution of the lowest-order mode of a triangular PCF. The specific mode is for a PCF with a pitch, Λ, of 2.3 μm, and a hole size d/Λ of 0.23, where d is the air hole diameter. The experimentally obtained field distribution is for the PCF operating at $\lambda = 458$ nm. The corresponding contour plot of the calculated field is presented in Fig. 3b. The field was calculated using the method of localized basis functions, in the high-frequency regime, using 200 basis functions. The distribution is seen to have the same rotational symmetry of the PCF. The field barely extends beyond the first row of air holes surrounding the defect, so the high-index region within the first row of holes indeed acts as the core of the fiber.

A manifestation of the resemblance of triangular PCFs to step-index fibers appears clearly when regarding the group velocity dispersion (GVD) of the fundamental mode. In Fig. 4 we have illustrated this by plotting the frequency dependence of the GVD for index-guiding PCFs and equivalent step-index fibers chosen by matching their effective cladding indices in the low-frequency limit [26]. From the figure a very similar behavior of the GVD is observed. There is, however, one important feature separating the GVD of the two fiber types. For both fibers the GVD of the lowest-order mode can reach negative values. While step-index fibers, however, always support more than one guided mode in the relevant frequency range, PCFs may be designed to support only a single mode in the same interval.

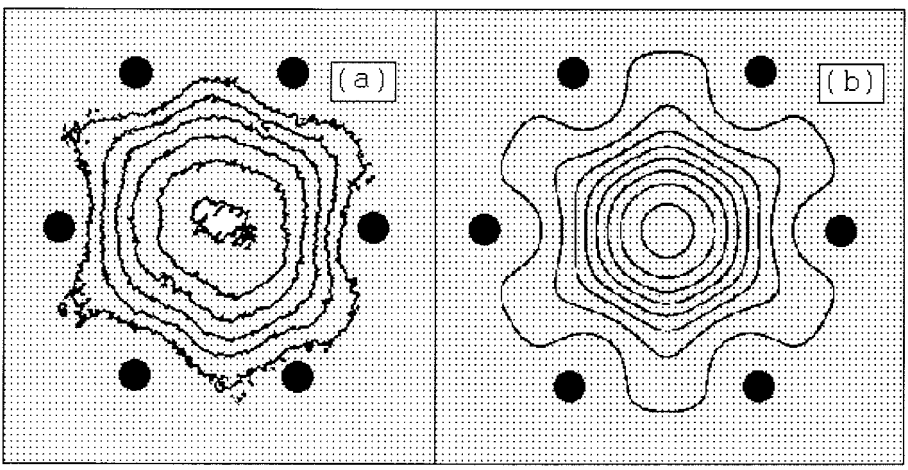

FIG. 3. Contour maps of the intensity distribution in the transversal plane of the observed (a) and modeled (b) lowest-order mode for $\lambda = 458$ nm. The spacing between the air holes is $\Lambda = 2.3$ μm, and the ratio of hole diameter to the spacing is $d/\Lambda = 0.23$. Filled circles represent the air holes closest to the defect.

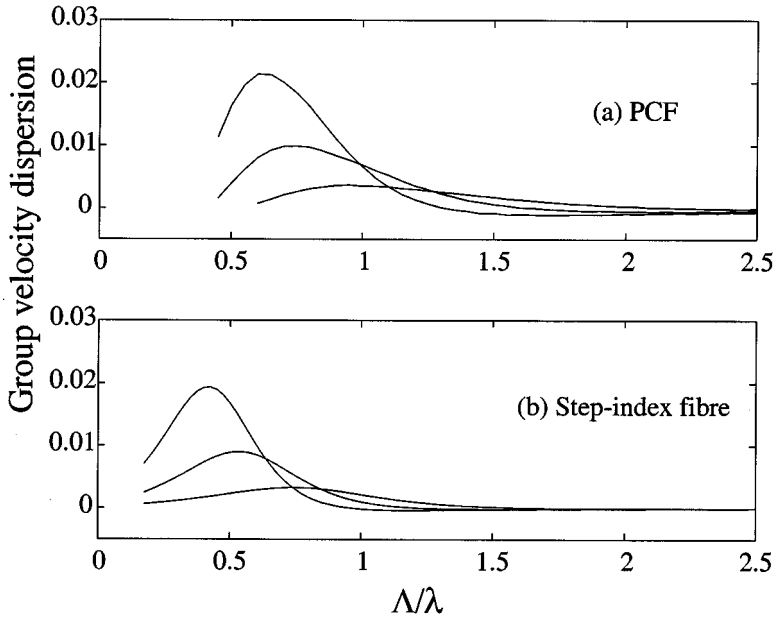

FIG. 4. Group velocity dispersion of the lowest-order mode of PCFs (a) and of equivalent step-index fibers with the diameter of the core equal to 2Λ (b). On both plots the curves correspond in descending order to $d/\Lambda = 0.45, 0.35, 0.25$. The plots represent a normalized waveguide dispersion $\partial^2(\beta\Lambda)/\partial(k\Lambda)^2$. Positive values of this quantity correspond to the normal conventional waveguide dispersion.

This makes the realization of PCFs having single-mode operation with negative GVD a realistic possibility.

In fact, the triangular PCFs may be designed for endlessly single-mode operation. This unique ability was first explained by Birks *et al.* using the effective-index approximation for the cladding structure [26] (see also Section IIA). In traditional fiber theory, a normalized frequency, V, is often used to determine the number of guided modes in step-index fibers [31],

$$V = \frac{2\pi\rho}{\lambda}\sqrt{n_{\text{co}}^2 - n_{\text{cl}}^2}, \tag{8}$$

where ρ is the core radius. Unlike for step-index fibers, the effective V value for PCFs tends to a stationary value in the high-frequency regime. This behavior is illustrated in Fig. 5 and is a result of the strong wavelength dependency of the photonic crystal cladding index. In the high-frequency limit, the effective index of the cladding n_{cl} is approaching n_{co} [26], and we therefore realize from (8) that a stationary V_{eff} value may be reached for the PCFs. This is, of course, in direct contrast to standard optical fibers, where the cladding index is largely wavelength independent, and $V \to \infty$ for $\lambda \to 0$, resulting in multimode operation.

The stationary V_{eff}-value is defined by the ratio of the hole diameter d to the period of the lattice Λ, and increases with the ratio. Thus by designing PCFs with d/Λ below a certain value, V_{eff} may be kept under the second-order mode cutoff

value over any wavelength range, thereby ensuring an endlessly single-mode operation. For step-index fibers this cutoff V value is 2.405, and although a different value is expected for the PCFs, we see from Fig. 5 that a cutoff V_{eff} of approximately 2.5 has been experimentally obtained. Above this V_{eff} value the triangular PCFs support higher-order modes, and a calculated field profile of the second-order mode is illustrated in Fig. 6. The profile is seen to be very similar to second-order modes of step-index fibers.

B. *Advanced Properties*

Among the most interesting aspects of the work on PCFs are of course their waveguiding properties with respect to their possible application in modern fiber optical communication and sensor systems. This means that a considerable interest is directed toward aspects such as spotsize behavior, loss properties, and dispersion properties. It is noteworthy that this area of investigation is still very young, and we must, consequently, expect that many new developments and more accurate methods for characterization and analysis will enter in the field. However, in order to get a first impression of some of the waveguiding properties of PCFs, we have chosen to apply the effective-index model (described in Section IIA) in an approximate analysis of the macrobending and dispersion properties of triangular PCFs.

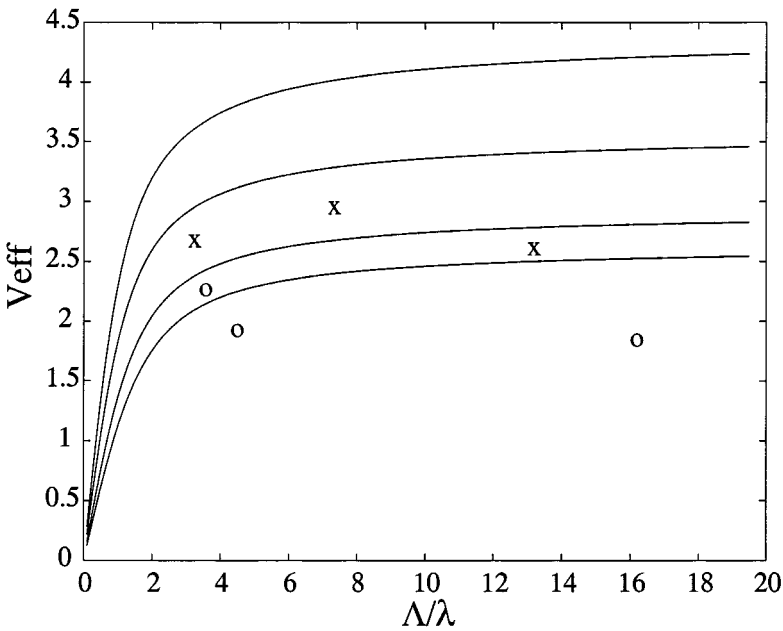

FIG. 5. V_{eff} for triangular high-index core PCFs. The curves correspond to values of $d/\Lambda = 0.45$, 0.35, 0.25, 0.2 in descending order. (X) Second-order-guided modes observed experimentally; (O) cases where the PCFs were found to support only the fundamental mode [22]. The measured contour map in Fig. 3a corresponds to the lowest-frequency (O) point.

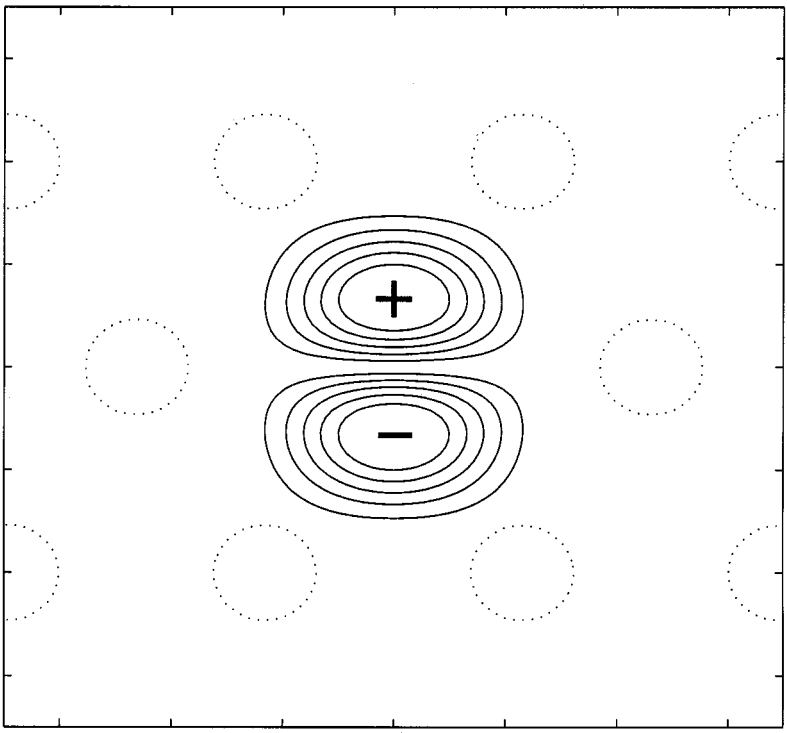

FIG. 6. Theoretical near-field contour plot of the second-order guided mode of a PCF with $d/\Lambda = 0.41$ and $\Lambda/\lambda = 4.8$. Similar to the fundamental mode, the field of the second-order mode is confined within the first row of holes represented as dotted circles.

B.1. *Bending losses.* The macrobending losses of optical fibers are very important, not only from a practical handling point of view, but also because they define the spectral window in which the fiber may be operated and provide important information about the modes of the fiber. In [26], the bending properties of the PCF were described by the introduction of a critical bend radius, i.e., a radius under which the fiber may not be bent in order for the excess bending loss to be below a given limit. However, in order to numerically characterize the unique PCF bending properties including both a low-wavelength and a long-wavelength bend-loss edge, we have here chosen to apply the bending loss formula described in [38]. In this formulation, which has proven to provide very accurate results for standard optical fibers, the power loss coefficient due to macrobending is written as

$$\alpha = \frac{\sqrt{\pi} A_e^2 a \exp\left(\dfrac{-4\Delta w^3}{3av^2} R\right)}{4Pw\sqrt{\dfrac{wR}{a} + \dfrac{v^2}{2\Delta w}}}, \tag{9}$$

where Δ is the relative index difference between the maximum refractive index in the core region and the cladding index, a is the core radius, v is the normalized

frequency, and w is the normalized decay parameter in the cladding. R is the radius of curvature, A_e is the amplitude coefficient of the cladding electric field, and P is the propagation power carried by the fundamental mode. Applying Eq. (9), we directly calculated the bend loss from the Bessel-function coefficients and propagation constant of the effective-index fiber. In order to choose a realistic bend radius in this analysis, we consider a situation where the full length of the fiber is coiled at a radius of 6.0 cm (corresponding to dispersion-compensating fiber coils, or coils in a laboratory). The bending-loss values for different air-hole dimensions are shown in Fig. 7 for a silica PCF with $\Lambda = 2.3$ μm. One of the most important observations is that both the upper and the lower bend edges are found, which clearly is in contrast to the case of the standard fiber. This difference is further illustrated in Fig. 7, where the bend loss is also shown for a standard fiber, which has the same core–cladding refractive-index difference as the PCF at the wavelength $\lambda = 1.3$ μm, and a core diameter of Λ. The bending loss results in Fig. 7 also indicate that a large operational wavelength range (of interest to optical communications) is available with PCFs. In addition, the PCFs have the perspective of providing very low scattering losses, because they may be fabricated from undoped silica, and as long as the air holes may be manufactured with sufficiently large diameters, the PCFs seem considerably more bending resistant than standard optical fibers.

B.2. *Dispersion.* If applications of PCFs are considered within the area of optical communication systems, then the most interesting question at present will probably be, What are the dispersion properties of the PCFs? In order to get closer to the answers to this question, the dispersion properties have been calculated using the effective-index model outlined in Section IIA. Once more, the design outlined in [26], i.e., a PCF with a pitch of 2.3 μm, is used as a point of reference.

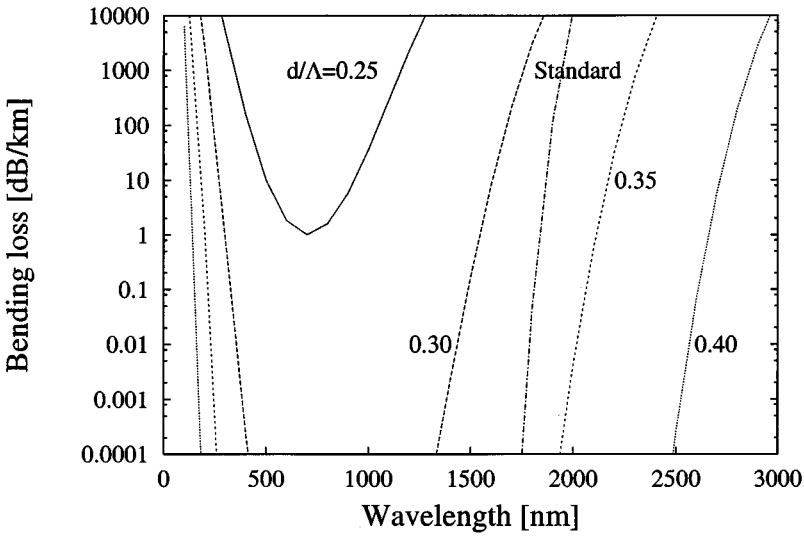

FIG. 7. Bending loss properties for standard fiber and PCFs coiled with a 6.0 cm radius. The numbers indicate the relative air-hole diameter d/Λ. Similar results have been presented in [27].

For such fibers with variable air-hole filling fractions, the calculated dispersion is shown in Fig. 8 as a function of wavelength.

From Fig. 8, we first note that for very small air filling fractions, e.g., when the influence of the air holes is strongly limited, the dispersion curve is expectedly very close to the material dispersion of pure silica (zero dispersion wavelength around 1.3 μm). As the diameter of the air holes is increased, the waveguide dispersion becomes increasingly strong, and we obtain a significantly reduced dispersion. It is particularly interesting that an almost constant dispersion level around -60 ps/km/nm is predicted for a ratio $d/\Lambda = 0.40$. Note also that the wavelength range (over which the flattened dispersion is calculated) is very broad, and with reference to Section IIIB.1, the bending loss properties are not considered to be a serious limit. These dispersion results indicate the interesting possibility of applying the PCFs as dispersion-compensating or dispersion-managed fibers for optical communication systems. Therefore, to investigate this option further, a number of different designs have been analyzed. The most spectrally constant dispersion values were calculated for fibers with relative air-hole sizes around $d/\Lambda = 0.40$. Some of the results are presented in Fig. 9, where very flat dispersion curves with values below -100 ps/km/nm are seen.

For the fiber parameter range used in Fig. 9, it is noteworthy that the effective normalized frequency [26], V_{eff}, is in the range from 2.0 to 3.5 (smallest value for smallest pitch). This should be compared to the result of Knight *et al.* [22] (see also Fig. 5), who found that a PCF with $V_{\text{eff}} < 2.5$ could be expected to support only a single mode. Although based on an approximate numerical method, the dispersion results strongly indicate that PCFs have potential applications as dispersion-managing components, and we aim to address the issue of dispersion properties in much more detail in future work.

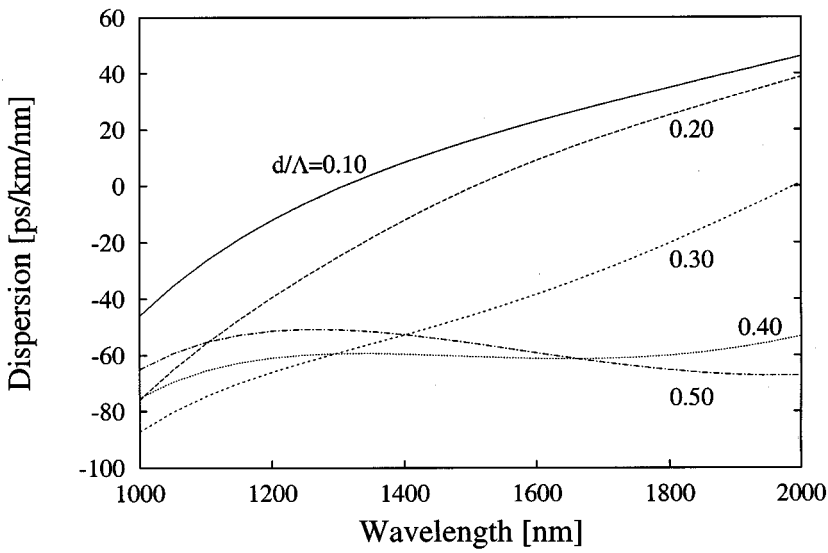

FIG. 8. Dispersion as a function of wavelength for PCFs with a fundamental cell diameter $\Lambda = 2.3$ μm (curves are shown for different ratios d/Λ). Similar results have been presented in [27].

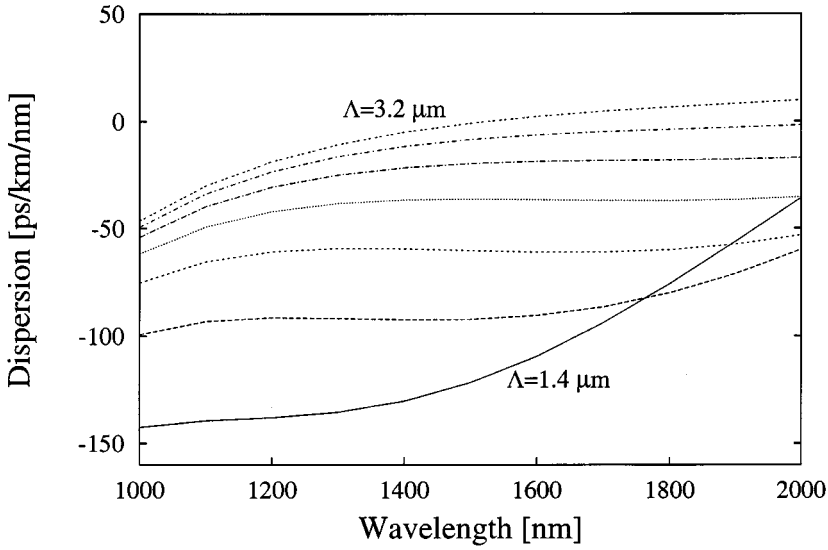

FIG. 9. Dispersion as a function of wavelength for PCFs with a relative hole size of $d/\Lambda = 0.40$ (curves for different pitch values: 1.4–3.2 μm in steps of 0.3 μm). Similar results have been presented in [27].

IV. WAVEGUIDING BY THE PBG EFFECT

The PCFs we have been investigating so far have all had the common characteristic of a high-index core and an operation based on TIR. In the remainder of this paper, we address a radically new concept for optical fibers, namely photonic bandgap guiding PCFs. For an understanding of the principle of waveguiding by the PBG effect, and as a basis for the analysis of the novel PCF, we first briefly touch upon some general aspects of photonic crystals and their classification.

A. *What Is a Photonic Bandgap?*

To support a full 3D PBG, that is the photonic crystal does not allow any modes within a band of frequencies to propagate, irrespectiple of direction, the crystal needs a full 3D periodicity [10, 39, 40]. However, structures with a 1D and 2D periodicity are also generally classified as photonic crystals [41–43]. Where the 1D case is well known and has been exploited for many years, finding use in, e.g., high-reflective mirrors, the possibilities of utilizing 2D periodic structures for achieving PBGs have only been realized within the past decade. The main reason for this is that where any refractive index contrast between the different layers in a 1D periodic structure results in a 1D forbidden gap, the realization of 2D PBGs is far more demanding. The realization requires both a relatively large refractive index contrast and a properly designed wavelength-scale periodic microstructuring of the material. Such a periodic structuring at the wavelength scale represents today the major technological difficulty for the realization of 2D and 3D photonic crystals operating at optical frequencies.

A.1. *3D field propagation in 2D photonic crystals.* For 2D photonic crystals, with wave propagation restricted to the periodic plane, the electromagnetic fields may be decomposed into separate TE and TM components. While the low-index contrast between silica and air does not allow for overlapping PBGs for TE- and TM-polarized waves, it is important to notice that for the case of true 3D field propagation in 2D silica/air structures, full PBGs may open up [20]. In this quasi-3D case a separation of the fields in TE and TM components is no longer valid, and when using the term PBG in connection with the PCF investigations, we refer to a PBG common to all polarizations [44, 45].

For 2D photonic crystals (including quasi-3D cases such as for the photonic crystal fibers) the vectors describing the 2D lattice have no component out of the periodic plane. For 3D field propagation in a 2D structure (i.e., quasi-3D case) the out-of-plane component of the wave propagation vector, β, will therefore always remain constant. This knowledge of a well-defined out-of-plane component of the wave propagation vector for a fixed frequency mode is crucial for the analysis of the PBG guiding PCF. In the analysis, we operate with a normalized out-of-plane propagation wave vector component, $\beta\Lambda$ (normalized propagation constant), and normalized frequencies, $k\Lambda$, where again Λ is the distance between the nearest holes and k the free-space wave constant ($= 2\pi/\lambda$).

B. *Improved Cladding Structures: Honeycomb-Based Photonic Crystals*

Although the high-index core in triangular PCFs will always result in a fundamental mode guided by TIR, it is possible for higher-order modes to be PBG guided, requiring that the cladding structure exhibit the PBG effect. Until now, however, no such PBG-guided modes have been observed in triangular PCFs, and we have turned, therefore, our interest toward new cladding structures, in a search of photonic crystals exhibiting PBG effect at realizable dimensions. A structure that has proven superior to triangular structures, with respect to broader PBGs, is the honeycomb, or graphite, structure [24, 46, 47]. The honeycomb structure is illustrated in Fig. 10, along with an indication of Λ and the unit cell of the structure. As shown in Fig. 10, the air filling fraction, f, defined as the total area of the air holes in a unit cell relative to the total unit cell area, will not be the same for a triangular and a honeycomb structure with similar Λ and air-hole size. When comparing triangular and honeycomb structures and using f to describe the structures, it is, therefore, important to notice that for the same Λ and hole size, the honeycomb structure has a factor $2/3$ smaller f value.

A band-structure calculation using the plane-wave method for a honeycomb structure with an air filling fraction of 30% at a fixed β value of $2\pi/\Lambda$ is illustrated in Fig. 11. The band diagram reveals the existence of two PBGs (primary and secondary gaps). For the specific β value, no modes are allowed to propagate in the honeycomb photonic crystal if their frequencies fall within one of the two PBGs. To exemplify how to perform designs from the normalized parameters obtained from, e.g., the band diagram in Fig. 11, we chose a nearest hole distance, Λ, of 2 μm. For this value, the lower PBG region boundary of the primary gap ($k\Lambda = 4.75$) corresponds to the free-space wavelengths $\lambda = 2.65$ μm.

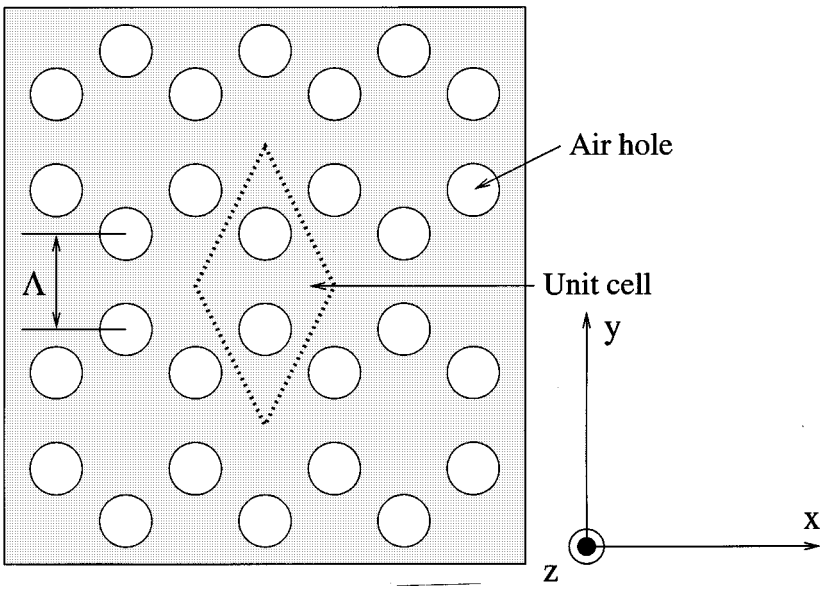

FIG. 10. The two-dimensional honeycomb PBG structure.

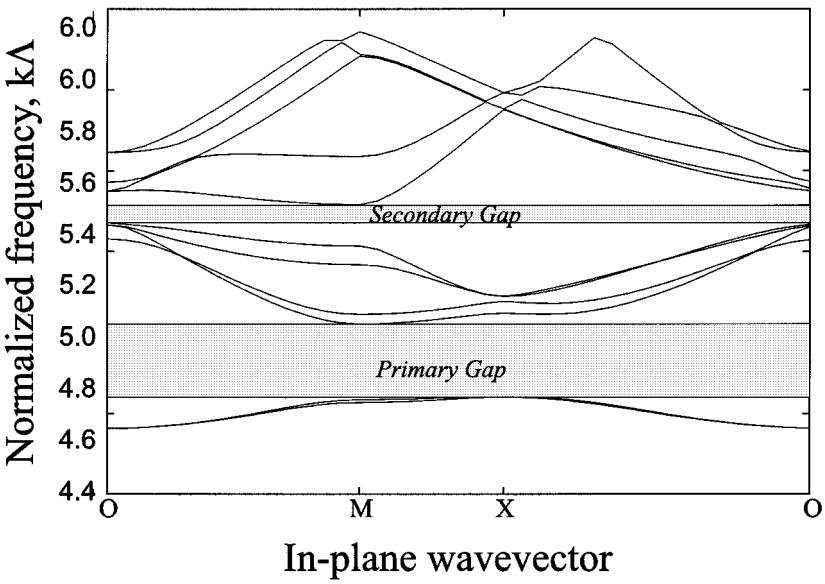

FIG. 11. Band-structure calculation for a honeycomb photonic crystal with an air filling fraction of 30% and out-of-plane wave-vector component fixed at $2\pi/\Lambda$. The three high symmetry points of the honeycomb crystal lattice are indicate by O, M, and X. For a full characterization of the photonic bandgaps of the crystal it is sufficient to sweep the in-plane component of the wave propagation vector along the boundaries of the irreducible Brilloin zone of the lattice [32].

By varying the β value and plotting the boundaries of the two bandgaps, the result in Fig. 12 is obtained. As is shown in the figure the silica/air photonic crystal does not exhibit any forbidden gaps in the pure 2D case ($\beta\Lambda = 0$); however, as $\beta\Lambda$ is increased (moving out of the plane) forbidden regions do open up. In the figure, we have introduced the ''radiation line'' defined as the envelope of the lowest-frequency-allowed mode (i.e., the fundamental space filling mode of the structure).

For the further analysis of honeycomb-based cladding structures, we include an investigation of the effect of adding small interstitial holes in the cladding structure. Such interstitial holes have been observed remaining in the cladding of recent PCFs, and attributed to the stack-and-pull fabrication technique of the PCFs [48]. In Fig. 13 we have illustrated the unit cells that were used, both for the study of triangular structures (Fig. 13a) and for honeycomb structures modified by interstitial holes (Fig. 13b). The relative size of the two gaps of the honeycomb structure with $f = 30\%$ is illustrated in Fig. 14. The relative size is defined as the width of the gap relative to its center frequency. Included also is the relative size of the first PBG appearing for a triangular structure with same air-hole sizes ($f = 45\%$). As seen, the relative size of the PBGs for the honeycomb structures is considerably larger than for the corresponding triangular structure. Furthermore, the interstitial holes are seen to increase the size of the PBGs, where in triangular structures these have been found to decrease the PBGs [24]. Building on the intuitive ideas of Joannopoulos *et al*. [3], where the broadest complete PBGs were found for structures with large nodes connected by thin veins (see Fig. 15), we realize the superiority of the honeycomb structure over the triangular structure. The honeycomb structure has intrinsically larger nodes and relatively narrower veins than the

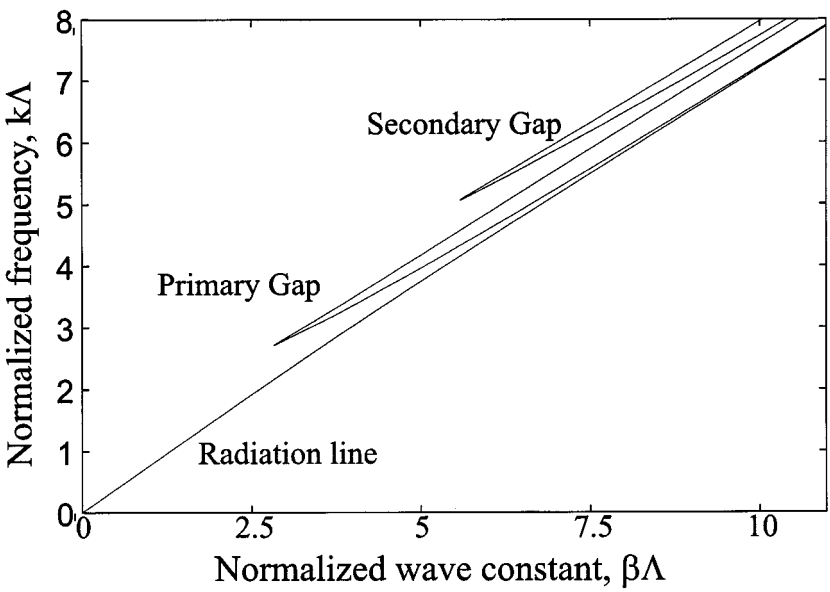

FIG. 12. Out-of-plane properties of a honeycomb photonic crystal with an air filling fraction of 30%. Two complete gaps are seen to open up above the radiation line, defined as the frequency of the fundamental space filling mode.

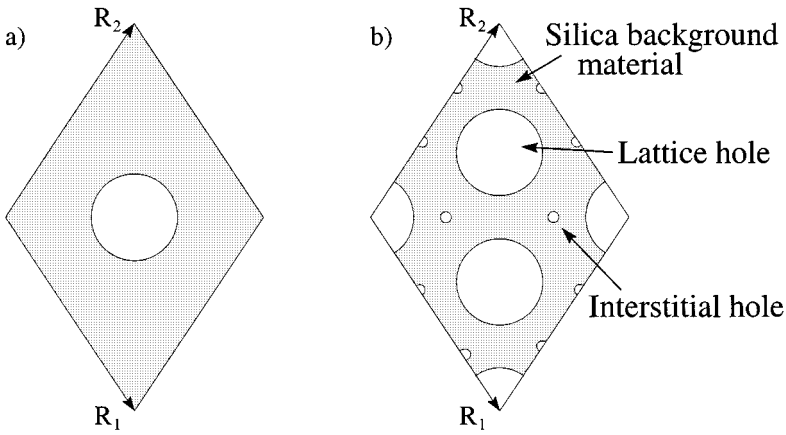

FIG. 13. (a) Unit cell employed for the study of triangular photonic crystals. The angle between the two lattice vectors $\mathbf{R_1}$ and $\mathbf{R_2}$ is 120°. (b) Unit cell employed for the general study of photonic crystals with a hexagonal symmetry. A honeycomb structure with interstitial holes results from setting the radius of the corner holes to zero.

triangular structure. Furthermore, for the triangular structure, we notice that the interstitial holes fall right in the center of the nodes (thereby severely damaging their ability to act as high-index centers); in contrast, the interstitial holes in the honeycomb structure are seen to leave the nodes undisturbed, while at the same time narrowing the veins even further.

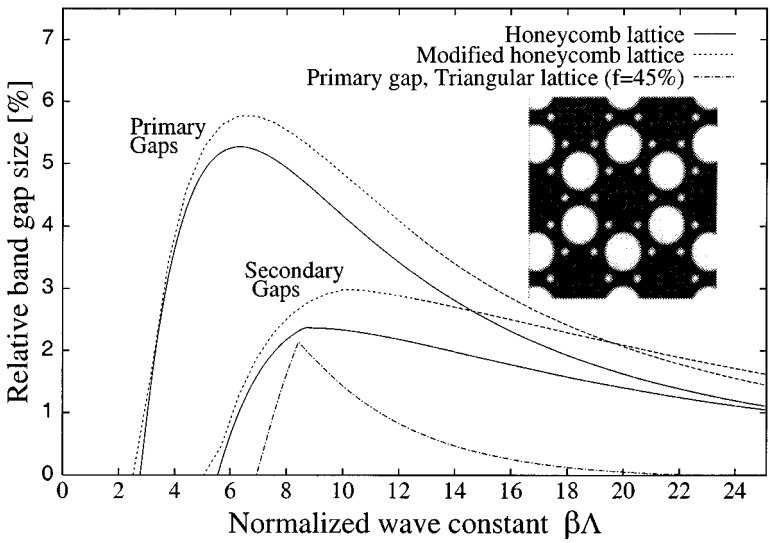

FIG. 14. Relative size of the photonic bandgaps for a honeycomb lattice with filling fraction $f = 30\%$. Interstitial holes are seen to have the effect of increasing the bandgaps. The insert shows the geometry of the honeycomb lattice with interstitial holes ($f_{\text{int}} = 5\%$, $f_{\text{tot}} = 50\%$). Similar results have been presented in [24].

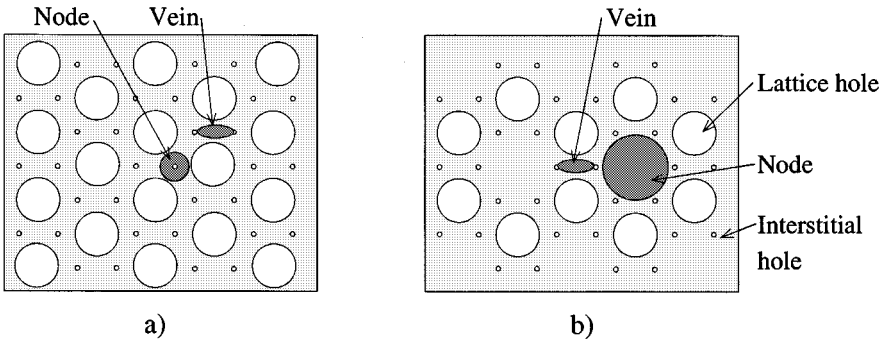

FIG. 15. Schematic illustration of the concept of nodes and veins for an intuitive understanding of the influence of interstitial holes in triangular structures (a) and honeycomb structures (b).

The investigations of cladding structures presented thus far have been for relatively large f values, where the triangular structures exhibit the PBG effect. However, apart from the broader PBGs, the honeycomb structures also exhibit the PBG effect at much lower f values than the triangular structures. This may prove vital for the realization of the novel fiber. We have found complete PBGs in honeycomb structure for f values down to as low as 5%, where no PBGs exist for triangular structures. We therefore conclude that at realizable air-hole sizes, the PBG effect is exhibited for honeycomb photonic crystals, and thus the basic requirement for obtaining confinement by this new physical mechanism may be fulfilled.

C. *Novel PCF Design*

Based on the results from the investigations of honeycomb-based cladding structures, we have recently proposed a novel PCF design operating solely by the PBG effect [24]. A cross-sectional schematic of the honeycomb-based PCF is illustrated in Fig. 16, along with the design of the high-index core triangular-based PCFs. Apart from the improved cladding structure it is seen to have a low-index centrally placed structural defect. This defect is easily introduced as an extra air hole with a size of the same order as the remainder of air holes. The exhibition of the PBG effect at realistic fabrication parameters is, of course, a fundamental prerequisite for obtaining PBG guidance, but the low-index defect proves further advantageous for studies of PBG guidance, as it does not allow a fundamental mode guided by TIR. An important feature of the new PCF is that it provides an extra degree of design freedom compared to triangular PCFs. For triangular PCFs only the pitch, the cladding hole sizes, and their shapes may be tuned for obtaining specific guiding properties. Since the core in these PCFs is simply created by a missing air hole, its geometry will be fixed by the above properties. In addition to the parameters of the triangular PCFs, the novel PCF further offers the possibility of varying the size and the shape of the central air hole, independently of the other fiber parameters. In Section IVD we shall demonstrate how the guided modes of the novel PCF may be affected by such changes.

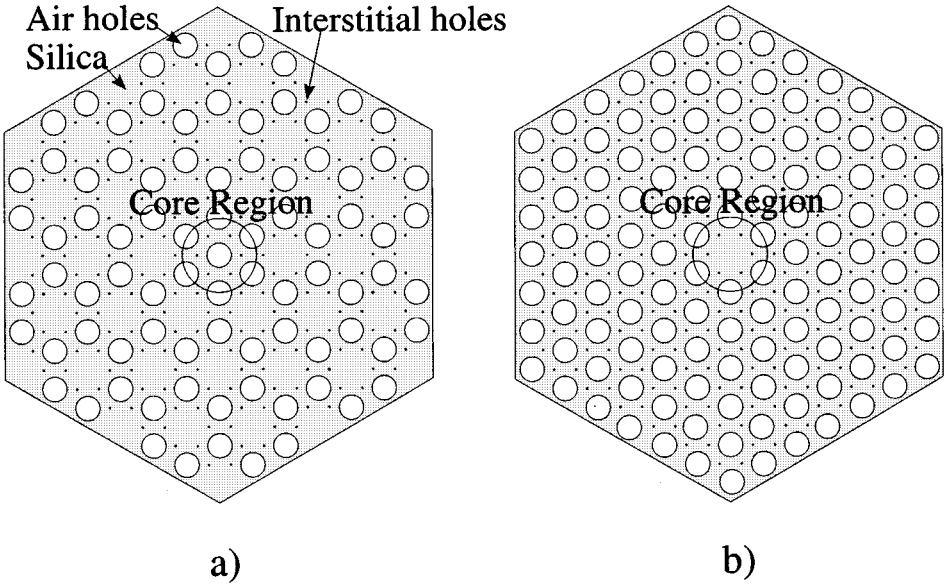

FIG. 16. (a) Cross-sectional view of a honeycomb photonic crystal fiber. For light having a frequency within the PBG of the surrounding cladding structure, the central periodicity-breaking region may act as a defect site, to which light can be confined. If the light has a nonzero wave-vector component in the direction of the fiber axis, it may thus be guided along the defect. (b) Cross-sectional view of a triangular photonic crystal fiber. The central defect here causes a high-index region to allow waveguiding by total internal reflection.

D. *Confinement of Light at Low-Index Defects: PBG Waveguidance*

For an easy-to-grasp explanation of the mechanism of confining light by the PBG effect, we consider a light source at a structural defect in a photonic crystal. The light source is operating at a fixed frequency falling inside the forbidden gap of the corresponding perfect photonic crystal. In the close vicinity of the defect the light does not experience the periodicity of the photonic crystal (the periodicity is, of course, broken at the defect), and the light may well be allowed as the PBG effect locally is not exhibited. Propagating away from the defect, the light starts experiencing the full periodic nature of the photonic crystal and will be expelled by the PBG effect, and thus forced back to the defect site. In this way a very strong confinement of the light around the defect site may be achieved, and the light will only be allowed to propagate if this takes place in the close vicinity of the defect site. Such PBG confinement has for planar structures (pure 2D case) theoretically been shown to result in extraordinary optical waveguides, with lossless transmission around sharp 90° degree bends [5, 9]. For the novel fiber a point defect, such as the central air hole, allows for modes with a frequency falling inside the PBG of the cladding structure to be guided along the defect in the direction perpendicular to the periodic plane, i.e., along the fiber axis.

To determine the guided modes of the honeycomb PCF, we employed a so-called supercell enhancement to the plane-wave method. This enhancement allows the treatment of structural defects in the photonic crystal. The principle for the

enhancement is simple, as it just includes representing the structure by a large unit cell in which the defect is included. The real problem that is solved is thus a periodic structure, where also the defect is repeated periodically. For the accurate calculation of the defect modes it is therefore necessary to choose a supercell sufficiently large that the spacing between the two nearest defects is large enough for their coupling to become negligible [33]. For the analysis of the honeycomb PCF we are operating with a supercell resulting in a spacing between two nearest defects of five simple honeycomb lattice vectors. Using the supercell plane-wave calculation with a basis of 2905 plane waves, the modal dispersion curves, illustrated in Fig. 17, were obtained. The calculation is for a honeycomb fiber with $f = 18\%$, a central air-hole diameter of 65% of the cladding holes, and no interstitial holes. The figure reveals several important differences between the novel fiber and conventional fiber, including the high-index core PCFs. First, no modes above the radiation line are observed, proving that no modes will be guided by total internal reflection in the novel design. For index guiding fibers, confinement is only achieved for modes having an effective index below the index of the core region and above the index of the cladding region (the radiation line). Considering first conventional fibers, a continuum of modes are allowed below the radiation line; however, as these modes are not confined to the core region but represent allowed cladding modes, a real fiber will not serve as a waveguiding structure for these modes. For the novel fiber, however, we see forbidden regions opening up below the radiation line, a phenomenon uniquely caused by the

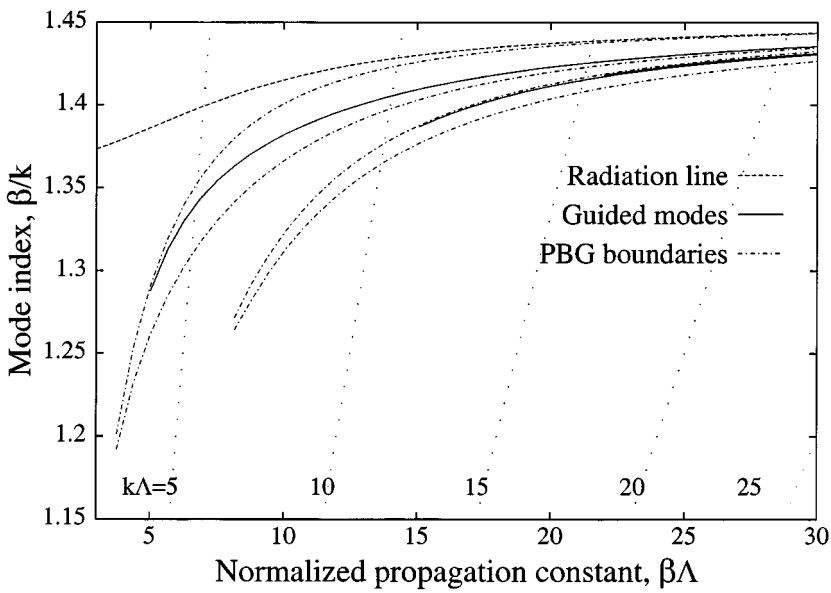

FIG. 17. Core modes of a honeycomb PCF. The top dashed curve is the radiation line, illustrating the effective refractive index of the cladding. The solid curves show the guided core modes. The dash−dotted curves surrounding the guided modes represent the PBG boundaries. Constant frequency lines (dotted) are also illustrated, with their respective values given at the lower part of the figure. Similar results have been presented in [49].

periodic structuring of the cladding. In these regions no modes are allowed in the full periodic photonic crystal, as discussed earlier, but the introduction of the central defect may cause the existence of localized defect modes. Indeed a doubly degenerate mode is seen to enter into the primary forbidden region at approx. $\beta\Lambda = 5$ and remains there until approx. $\beta\Lambda = 30$. At $\beta\Lambda$ around 15, a second mode is seen to enter the secondary bandgap. Single-mode operation of this specific PCF therefore may be achieved for $\beta\Lambda = 5$ to 15. For a PCF with $\Lambda = 2.0$ μm this interval corresponds to $\lambda = 1.2–3.2$ μm. We have found all the defect modes that are positioned inside the forbidden region to be localized to the low-index defect region. Moving to the PBG boundaries the modes start coupling to the allowed cladding modes, and these now-resonant defect modes therefore will not be supported by the PCF waveguide over long distances. Sharp transmission spectra for the PBG-guiding PCFs are therefore expected. As the defect modes move to the center of the PBG regions a very tight confinement around the low-index region is observed.

In Fig 18 we have plotted the calculated field distribution for the defect mode appearing in the primary PBG at $\beta\Lambda = 10$. As shown in Fig. 18 the field is strongly localized around the low-index core region. Although peak intensity appears outside the air region, this confined mode is fundamentally different to any guided modes in high-index fibers. In principle, even strong localization in the air regions of PBG-guiding PCFs is possible, and the prospects of this are clearly very appealing; e.g., for sensor applications, the ability to confine light in air regions will

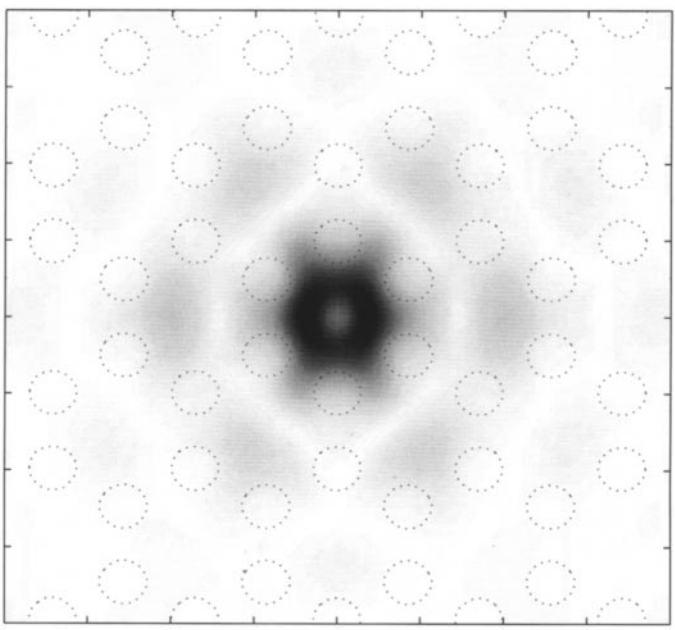

FIG. 18. Field distribution of a mode positioned in the primary PBG of the cladding. The real space hole structure around the fiber core is indicated by dotted circles. A strong confinement to the low-index core region is observed (dark regions represent high intensity). Similar results have been presented in [49].

open up sensing possibilities that cannot be achieved by today's known fiber types. Also for telecommunications applications, localization of part of the guided mode in air (or vacuum) regions may prove very interesting. It is clear that nonlinear effects may dramatically be reduced by the realization of a pure silica fiber, where a large portion of the field is guided in vacuum. Regarding nonlinear effects as setting the ultimate limits for the operation of today's fibers, it is clear that PBG-guiding PCFs have the potential to break the today known limitations. As the results presented in this paper only represent the first efforts to explore the potential of these new fibers, much work remains before they may find their way to practical applications. An important feature to determine is the dispersive properties of the PBG-guiding PCFs. We expect from the different waveguiding mechanism that these will be significantly different from index-guiding fibers. Although not directly presented in this paper, we may gain some knowledge of the dispersion in the honeycomb fibers from Fig. 17. First, it is seen that the modal index range in which the fibers may be operated is greatly widened compared to that of conventional fibers. As conventional fibers operate by TIR, this range is limited by the core and cladding index difference. However, for the PBG-guiding PCFs we see a much larger modal index range to operate in. Second, since the dispersion of the novel fiber may be viewed as the curvature of the modal index curve, we realize that the enlarged modal index range correspondingly greatly enlarges the possibilities of operating the novel PCF in a region with specifically tailored dispersive properties. Therefore, an obvious potential application of the novel PCFs will be as dispersion managing components.

Finally, we focus on the appealing high flexibility of the novel fiber. By the photonic bandgap effect, it is, as demonstrated, possible to open up forbidden regions by correctly microstructuring the cladding and by introducing a defect site to localize light within this region. By independently optimizing the cladding and the defect structures, it is thus possible to tailor the properties of the fiber. In Fig. 19 we have illustrated that it is possible by varying the size of the central defect hole, but keeping the cladding structure fixed, to precisely tune the frequency of the defect mode within the PBG region of the cladding. Although we have only been investigating defect sites introduced by a single additional air hole, many other ways of creating such defects may be thought of; e.g., for polarization-managing purposes the introduction of asymmetric defects (possibly with a larger defect region than that presented here) seems intuitively a correct design route. In future work, we will aim at addressing such more sophisticated PBG-guiding PCFs.

V. SUMMARY

In this paper we have reviewed some of the progress in the field of photonic crystal fibers. Emphasis has been on the applicational aspects of high-index core triangular photonic crystal fibers, and qualitative results on their single-mode operation, bending losses, and dispersive properties have been presented. We have been investigating the basic guiding properties of a new class of optical fibers, which are radically different from all known fibers of today, and are operating

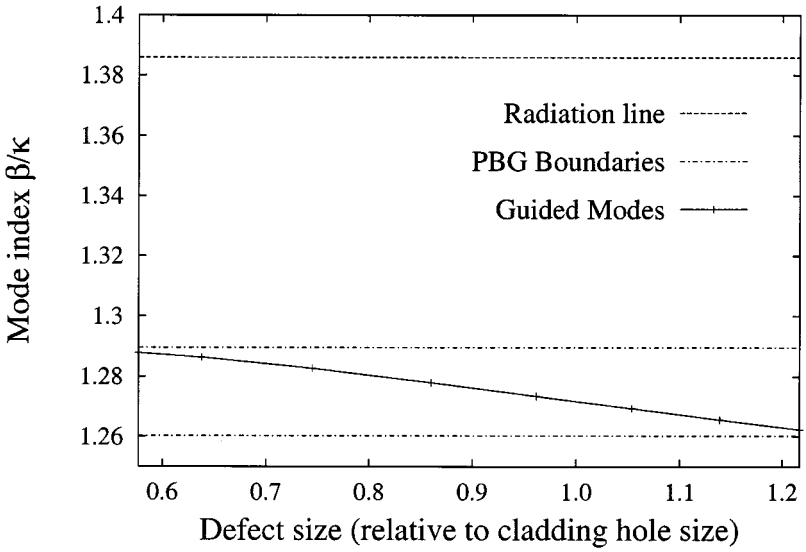

FIG. 19. Tuning of the frequency of the core mode precisely within the PBG by varying the size of the central hole. The plot is for a fixed value of $\beta\Lambda = 5$.

solely by the photonic bandgap effect. The prospects of having a fundamentally new way of guiding light, completely different from that exploited for several decades now in conventional optical fibers, seem extremely interesting and we have briefly touched upon some of the new possibilities offered by the novel fibers. While the results presented in this paper represent the first efforts to explore the potential of these new fibers, much work remains for determining their potential use in specific applications, and we will pursue this in more detail in our future work.

ACKNOWLEDGMENTS

Professor Philip St. J. Russel, Dr. Jonathan C. Knight, and Dr. Tim A. Birks are acknowledged for fruitful discussions. This work was supported by the Danish Technical Research Council under the THOR (Technology by Highly Oriented Research) program.

REFERENCES

[1] A. Bjarklev, *Optical Fiber Amplifiers: Design and System Application*, Artech House, Boston/London, 1993.

[2] E. Yablonovitch, "Inhibited spontaneous emission in solid-state physics and electronics," *Phys. Rev. Lett.*, vol. 58, 2059 (1987).

[3] J. D. Joannopoulos, J. N. Winn, and R. D. Meade, *Photonic Crystals: Molding the Flow of Light*, Princeton Univ. Press, Princeton, 1995.

[4] P. St. J. Russell, D. M. Atkin, and T. A. Birks, "Bound modes of two-dimensional photonic crystal waveguides," *Quantum Optics in Wavelength Scale Structures*, 1996.

[5] A. Mekis, J. C. Chen, I. Kurland, S. Fan, P. R. Villeneuve, and J. D. Joannopoulos, ''High transmission through sharp bends in photonic crystal waveguides,'' *Phys. Rev. Lett.*, vol. 77, 3787 (1996).

[6] H. Benisty, ''Modal analysis of optical guides with two-dimensional photonic band-gap boundaries,'' *J. Appl. Phys.*, vol. 79, 7483 (1996).

[7] P. R. Villeneuve, S. Fan, and J. D. Joannopoulos, ''Microcavities in photonic crystals: Mode symmetry, tunability, and coupling efficiency,'' *Phys. Rev. B*, vol. 54, 7837 (1996).

[8] S. Fan, J. N. Winn, A. Devenyi, J. C. Chen, R. D. Meade, and J. D. Joannopoulos, ''Guided and defect modes in periodic dielectric waveguides,'' *J. Opt. Soc. Am. B*, vol. 12, 1267 (1997).

[9] R. W. Ziolkowski, ''Fdtd modelling of photonic nanometer-sized power splitters and switches,'' in *Integrated Photonics Research*, *Technical Digest Series*, vol. 4, ITuA2, OSA, Mar.–Apr. 1998.

[10] E. Yablonovitch, ''Photonic band-gap structures,'' *J. Opt. Soc. Am. B*, vol. 10, 283 (1993).

[11] S. John, ''Localization of light: Theory of photonic band gap materials,'' in *Photonic Band Gap Materials*, (C. M. Soukoulis, Ed.), pp. 563–666, *NATO ASI Series: Series E, Applied Sciences*, vol. 315, NATO Scientific Affairs Division, Kluwer, Dordrecht, 1996.

[12] T. F. Krauss, R. M. De La Rue, and S. Brand, ''Two-dimensional photonic-bandgap structures operating at near-infrared wavelengths,'' *Nature*, vol. 383, 699 (1996).

[13] T. Baba and T. Matsuzaki, ''Polarisation changes in spontaneous emission from GaInAsP/InP two-dimensional photonic crystals,'' *Electron. Lett.*, vol. 31, 1776 (1995).

[14] P. W. Evans, J. J. Wierer, and N. Holonyak, ''Photopumped laser operation of an oxide post gaas-alas superlattice photonic lattice,'' *Appl. Phys. Lett.*, vol. 70, 1119 (1997).

[15] O. Painter, J. O'Brian, R. Lee, C. C. Cheng, B. D'Urso, A. Yariv, and A. Scherer, ''Lasers incorporating two-dimensional photonic crystal mirrors,'' in *CLEO'97*, p. CFQ2, May 1997.

[16] S. L. McCall, P. M. Platzman, R. Dalichaouch, D. Smith, and S. Schultz, ''Microwave propagation in two-dimensional dielectric lattices,'' *Phys. Rev. Lett.*, vol. 67, 2017 (1991).

[17] S. D. Cheng, R. Biswas, E. Özbay, S. McCalmont, G. Tuttle, and K.-M. Ho, ''Optimized dipole antennas on photonic band gap crystals,'' *Appl. Phys. Lett.*, vol. 67, 3399 (1995).

[18] M. P. Kesler, J. G. Maloney, B. L. Shirley, and G. S. Smith, ''Antenna design with the use of photonic band-gap materials as all-dielectric planar reflectors,'' *Microwave Opt. Technol. Lett.*, vol. 11, 169 (1996).

[19] T. A. Birks, D. M. Atkin, G. Wylangowski, P. St. J. Russell, and P. J. Roberts, ''2d photonic band gap structures in fibre form,'' in *Photonic Band Gap Materials*, (C. M. Soukoulis, Ed.), Kluwer, Dordrecht/Norwell, MA, 1996.

[20] T. A. Birks, P. J. Roberts, P. St. J. Russell, D. M. Atkin, and T. J. Shepherd, ''Full 2-d photonic bandgaps in silica/air structures,'' *Electron. Lett.*, vol. 31, 1941 (1995).

[21] J. C. Knight, T. A. Birks, P. St. J. Russell, and D. M. Atkin, ''All-silica single-mode optical fiber with photonic crystal cladding,'' *Opt. Lett.*, vol. 21, 1547 (1996).

[22] J. C. Knight, T. A. Birks, P. St. J. Russell, and J. P. Sandro, ''Properties of photonic crystal fiber and the effective index model,'' *J. Opt. Soc. Am. A*, vol. 15, 748 (1998).

[23] Homepage of the Optoelectronics Group, Department of Physics, University of Bath.

[24] J. Broeng, S. E. Barkou, A. Bjarklev, J. C. Knight, T. A. Birks, and P. St. J. Russel, ''Highly increased photonic band gaps in silica/air structures,'' *Opt. Commun.*, vol. 156, 240 (1998).

[25] J. Broeng, S. E. Barkou, and A. Bjarklev, ''Waveguiding by the photonic band gap effect,'' in *Topical Meeting on Electromagnetic Optics*, Marseille, 1998. EOS.

[26] T. A. Birks, J. C. Knight, and P. St. J. Russell, ''Endlessly single-mode photonic crystal fiber,'' *Opt. Lett.*, vol. 22, 961 (1997).

[27] A. Bjarklev, J. Broeng, S. E. Barkou, and K. Dridi, ''Dispersion properties of photonic crystal fibers,'' in *ECOC'98*, Madrid, Sept. 1998.

[28] D. Gloge, ''Weakly guiding fibers,'' *Appl. Opt.*, vol. 10, 2252 (1971).

[29] J. W. Fleming, ''Material dispersion in lightguide glasses,'' *IEE Electron. Lett*., vol. 14, 326 (1978).

[30] D. Mogilevtsev, T. A. Birks, and P. St. J. Russell, ''Dispersion of the photonic crystal fibres,'' *Opt. Lett*., vol. 23, 1662 (1998).

[31] A. W. Snyder and J. D. Love, *Optical Waveguide Theory*, pp. 595–606, Chapman and Hall, London, 1983.

[32] K. M. Ho, C. T. Chan, and C. M. Soukoulis, ''Existence of a photonic gap in periodic dielectric structures,'' *Phys. Rev. Lett*., vol. 65, 3152 (1990).

[33] R. D. Meade, A. M. Rappe, K. D. Brommer, J. D. Joannopoulos, and O. L. Alerhand, ''Accurate theoretical analysis of photonic band-gap materials,'' *Phys. Rev. B*, vol. 48, 8434 (1993).

[34] K. M. Leung, ''Defect modes in photonic band structures: A Green's function approach using vector wannier functions,'' *J. Opt. Soc. Am. B*, vol. 10, 303 (1993).

[35] J. B. Pendry, ''Photonic band structures,'' *J. Modern Opt*., vol. 41, 209 (1994).

[36] A. R. McGurn, ''Green's-function theory for row and periodic defect arrays in photonic band structures,'' *Phys. Rev. B*, vol. 53, 7059 (1996).

[37] J. G. Maloney, M. P. Kesler, B. L. Shirley, and G. S. Smith, ''A simple description for waveguiding in photonic bandgap materials,'' *Microwave Opt. Technol. Lett*., vol. 14, 261 (1997).

[38] J. Sakai and T. Kimura, ''Bending loss of propagation modes in arbitrary-index profile optical fibers,'' *Appl. Opt*., vol. 17, 1499 (1978).

[39] S. Fan, P. R. Villeneuve, R. D. Meade, and J. D. Joannopoulos, ''Design of three-dimensional photonic crystals at submicron lengthscales,'' *Appl. Phys. Lett*., vol. 65, 1466 (1994).

[40] N. Yamamoto, S. Noda, and A. Sasaki, ''New realization method for three-dimensional photonic crystal in the optical wavelength region: Experimental consideration,'' *Japanese J. Appl. Phys. 1*, vol. 36, 1907 (1997).

[41] J. P. Zhang, D. Y. Chu, S. L. Wu, W. G. Bi, R. C. Tiberio, R. M. Joseph, A. Taflove, C. W. Tu, and S. T. Ho, ''Nanofabrication of 1-d photonic bandgap structures along a photonic wire,'' *IEEE Photon. Technol. Lett*., vol. 8, 491 (1996).

[42] T. Baba and T. Matsuzaki, ''Theoretical calculation of photonic gap in semiconductor 2-dimensional photonic crystals with various shapes of optical atoms,'' *Japanese J. Appl. Phys. 1*, vol. 34, 4496 (1995).

[43] D. Labilloy, H. Benisty, C. Weisbuch, T. F. Krauss, R. Houdre, and U. Oesterle, ''Use of guided spontaneous emission of a semiconductor to probe the optical properties of two-dimensional photonic crystals,'' *Appl. Phys. Lett*., vol. 71, 738 (1997).

[44] A. A. Maradudin and A. R. McGurn, ''Out of plane propagation of electromagnetic waves in a two-dimensional periodic dielectric medium,'' *J. Modern Opt*., vol. 41, 275 (1994).

[45] X. P. Feng and Y. Arakawa, ''Off-plane angle dependence of photonic band gap in a two-dimensional photonic crystal,'' *IEEE J. Quantum Electron*., vol. 32, 535 (1996).

[46] D. Cassagne, C. Jouanin, and D. Bertho, ''Optical properties of two-dimensional photonic crystals with graphite structure,'' *Appl. Phys. Lett*., vol. 70, 289 (1997).

[47] A. Barra, D. Cassagne, and C. Jouanin, ''Existence of two-dimensional absolute photonic band gaps in the visible,'' *Appl. Phys. Lett*., vol. 72, 627 (1998).

[48] J. C. Knight, T. A. Birks, R. F. Cregan, and P. St. J. Russell, ''Photonic crystals as optical fibres—Physics and applications,'' *Opt. Mater*., in press.

[49] S. E. Barkou, J. Broeng, and A. Bjarklev, ''Silica-air photonic crystal fiber design that permits waveguiding by a true photonic bandgap effect,'' *Opt. Lett*., in press.